Journal of Catalysis 283 (2011) 98–107

Contents lists available at SciVerse ScienceDirect

Journal of Catalysis

journal homepage: www.elsevier.com/locate/jcat

Catalytic consequences of hydroxyl group location on the kinetics of *n*-hexane hydroisomerization over acidic zeolites

Hsu Chiang, Aditya Bhan *

Department of Chemical Engineering and Materials Science, University of Minnesota – Twin Cities, 421 Washington Avenue SE, Minneapolis, MN 55455, USA

ARTICLE INFO

Article history:
Received 12 April 2011
Revised 30 June 2011
Accepted 24 July 2011
Available online 30 August 2011

Keywords:
Alkane hydroisomerization
Zeolite
Mordenite
Bifunctional catalysis
Shape selectivity
Partial confinement
Entropy-driven reactions
Electrostatic stabilization

ABSTRACT

The measured kinetics of n-C_6H_{14} hydroisomerization reactions is consistent with a bifunctional mechanism involving the facile dehydrogenation of *n*-hexane on the metal catalyst and a kinetically relevant step involving isomerization of *n*-hexene on zeolitic acidic sites. The measured activation entropy in small 8-MR pockets of MOR (-35 J mol^{-1} K^{-1}) is similar to that in larger 12-MR channels of MOR (-37 J mol^{-1} K^{-1}) and BEA (-33 J mol^{-1} K^{-1}) but higher than that in medium pore FER (-86 J mol^{-1} K^{-1}), suggesting that partial confinement of C_6 olefinic reactants results in lower free energy for the isomerization reaction in 8-MR pockets of MOR. The hypothesis that a cyclopropane-like cationic transition state is not completely contained within the 8-MR pockets of MOR is consistent with the observed selectivity to 2-methylpentane and 3-methylpentane in the 8-MR pockets being identical to that measured in larger 12-MR channels of MOR and BEA. The lower activation energy measured in 8-MR pockets compared to larger 12-MR channels of MOR may arise due to greater electrostatic stabilization of the positively charged transition state by framework oxygen atoms located on the pore mouth of the smaller 8-MR pockets of MOR or due to the larger heat of adsorption caused by confinement in smaller 8-MR pockets. The lower activation energy in 8-MR channels and comparable loss in entropy mediated by partial confinement results in the rate per proton in 8-MR pockets being five times larger than the rate in 12-MR channels of MOR. These results provide another conceptual consideration for rigorous and quantitative understanding of local environment effects of zeolite channel size and connectivity on the rate and selectivity of acid-catalyzed reactions.

1. Introduction

The rates and selectivity of solid acid-catalyzed reactions are functions of the catalyst structure and acid strength. Since the acid strength of high-silica zeolites is almost invariant as assessed by calculations of the deprotonation energy (range: 1170–1200 kJ mol^{-1}) [1,2], reactions of hydrocarbons catalyzed by high-silica zeolites are mainly affected by the micropore structure [3–5].

The zeolite environment that circumscribes acidic OH groups can result in remarkable differences in catalytic rates and selectivities that have been broadly described by the term shape selectivity and its specific manifestations such as "active site shape selectivity" and "restricted transition state selectivity" [5,6]. Emerging research has particularly focused on the disparate OH group environments in 12- and 8-membered ring (MR) channels of MOR and the ability of OH groups in 8-MR channels to enable site specific catalysis for carbonylation of methyl groups and monomolecular dehydrogenation of alkanes as demonstrated in the recent work by Iglesia and co-workers [6–10]. We have shown that OH groups in 8-MR channels in MOR selectively dehydrate ethanol to ethylene because 8-MR pockets in MOR protect ethanol monomers from forming larger and more stable ethanol dimers due to size restrictions [11]. These recent examples in the literature demonstrate that hydroxyl groups circumscribed in smaller 8-MR channels of MOR catalyze reactions with rates and selectivity higher/different than in larger 12-MR channels of MOR for acid-catalyzed reactions mediated by charge, entropy, or size as specific considerations. In this work, we extend the scope of these recent reports to demonstrate the catalytic consequences of OH group environment on bifunctional *n*-hexane hydroisomerization reactions and quantitatively discern enthalpic and entropic drivers for this reaction.

Alkane hydroisomerization catalyzed by bifunctional metal–acid formulations is an important reaction in petrochemical refining for transforming linear saturated hydrocarbons to branched hydrocarbons with higher octane rating. The mechanism and kinetics of bifunctional hydroisomerization have been extensively studied on solid acid catalysts [12–14]; we use it here as a probe reaction to assess whether the same mechanism is prevalent on acidic sites in all zeolite environments and to quantitatively assess

* Corresponding author.
E-mail addresses: chian058@umn.edu (H. Chiang), abhan@umn.edu (A. Bhan).

0021-9517/$ - see front matter © 2011 Elsevier Inc. All rights reserved.
doi:10.1016/j.jcat.2011.07.006

how kinetic parameters within the proposed mechanism vary with OH group environment. The generally accepted pathway of hydroisomerization based on the study by Weisz and Swegler [15] includes dehydrogenation of the linear alkane to form a linear alkene on the metal surface. This linear alkene is isomerized into a branched alkene on the acidic site in the zeolite micropore environment; subsequently, this branched alkene is hydrogenated over the metal catalyst to generate a branched alkane. Alkane isomerization can be catalyzed by only the acidic zeolite, but high temperatures are required (573 K on zeolite BEA) [16] for initial dehydrogenation of the alkane, and in absence of H_2 and metal catalysts, high concentrations of alkenes result in excessive oligomerization, cyclization, and aromatization reactions that form unreactive carbon deposits [8,16–18]. In bifunctional catalyst formulations, however, because the equilibrium of alkane, alkene, and hydrogen is established by platinum at lower temperatures (~473 K), low concentrations of olefins are maintained by adjusting the alkane to H_2 ratio in the feed [18].

The detailed mechanism for how linear alkenes are transformed into branched alkenes over acidic zeolites has also been extensively studied by computational chemistry methods. Hybrid quantum mechanical–molecular mechanical (QM/MM) calculations show that surface-bound, linear alkoxide intermediates formed upon chemisorption are more stable than physisorbed linear alkenes [19,20] and that the stability of the linear alkoxide intermediate increases with increasing carbon number in FER (C_3–C_5) [19] and FAU (C_2–C_8) [20]. Linear alkoxide species have been observed as stable intermediates in ^{13}C NMR and infrared spectra during alcohol dehydration and protonation of alkenes on zeolite surfaces [21–23]. The isomerization of a linear alkoxide into a branch alkoxide occurs via an edge-protonated cyclo-propane species as a transition state which is energetically favored compared to directly shifting the alkyl group as shown by Demuth et al. [24] and Boronat et al. [25] using density functional theory (DFT).

In this study, three zeolite framework materials (H-BEA, H-FER, and H-MOR) were chosen to study the effects of zeolite pore connectivity, channel size, and location of OH groups on the rate and selectivity of *n*-hexane hydroisomerization over bifunctional catalysts consisting of physical mixtures of zeolites and Pt/Al_2O_3 (0.9–1 Pt/H^+ in molar ratio). The measured rate of isomerization over the three zeolite materials is a function of n-C_6H_{14}/H_2 (molar ratio), consistent with a bifunctional mechanism involving the facile dehydrogenation of *n*-hexane on the metal catalyst and a kinetically relevant step involving isomerization of *n*-hexene on zeolitic acidic sites. Zeolite BEA has the highest rate among the zeolites considered because it has lower activation energy than MOR and higher activation entropy than FER. The rate per proton in the 8-MR side pockets in MOR is five times higher than the rate in the 12-MR channels because the activation energy in 8-MR pockets is lower than that in 12-MR channels. The measured entropy of activation (-34.7 ± 9.8 J mol^{-1} K^{-1}) and selectivity to 2-MP and 3-MP (1.55:1) in the 8-MR pockets within MOR are similar to those in the 12-MR channels of MOR (-37.4 ± 9.7 J mol^{-1} K^{-1} and 1.5:1) and of BEA (-33.1 ± 4.3 J mol^{-1} K^{-1} and 1.35:1), suggesting that the *n*-hexene molecule is only partially confined in the 8-MR pockets of H-MOR.

2. Materials and methods

2.1. Catalyst preparation

FER (Si/Al = 11.5, CP 914c), MOR (Si/Al = 11.1, CBV 21A), and BEA (Si/Al = 12.0, CP 814 E) zeolite samples from Zeolyst, where the silicon to aluminum ratio (Si/Al) was determined by elemental analysis (Galbraith Laboratories), in their NH_4^+ form were sieved to maintain particle sizes between 180 and 425 μm (40–80 mesh) and subsequently treated in dry air (1.67 cm^3 s^{-1} at NTP conditions, ultrapure, Minneapolis Oxygen) to thermally decompose NH_4^+ to H^+ and $NH_{3(g)}$ by increasing the temperature from ambient to 773 K at 0.0167 K s^{-1} and holding for 4 h. The proton form FER, MOR, and BEA zeolite samples are abbreviated as H-FER, H-MOR, and H-BEA, respectively.

γ-Al_2O_3 (Sasol North America Inc., Lot # C1964, 189 m^2 g^{-1}, 0.44 cm^3 g^{-1} pore volume) was treated in flowing dry air (1.67 cm^3 s^{-1} at NTP conditions, ultrapure, Minneapolis Oxygen) to 923 K for 3 h (0.083 K s^{-1}) before adding the metal precursor. Pt/Al_2O_3 formulations (1.5 wt.% Pt) were prepared by the incipient wetness impregnation of γ-Al_2O_3 using chloroplatinic acid solution ($H_2PtCl_6{\cdot}6H_2O$, 99.95% (metal basis), Alfa Aesar) as precursor. After impregnation, samples (yellow in color) were treated in dry air (1.67 cm^3 s^{-1} at NTP conditions, ultrapure, Minneapolis Oxygen) at 383 K for 9 h and subsequently heated to 823 K (0.083 K s^{-1}) for 4 h to thermally decompose the precursors. After decomposing the precursor, the sample was treated in H_2 (3.3 cm^3 g^{-1} s^{-1}, ultrapure carrier grade, Airgas) at 723 K (0.083 K s^{-1}) for 2 h and then cooled to ambient temperatures in dry He flow (1.67 cm^3 s^{-1}, ultrapure, Minneapolis oxygen). The Pt cluster surface was passivated by treating Pt/Al_2O_3 formulations (black color) in mixtures of dry air (0.1–0.3 cm^3 g^{-1} s^{-1}, ultrapure, Minneapolis Oxygen) and He (3.3 cm^3 g^{-1} s^{-1}, ultrapure, Minneapolis oxygen) at 298–303 K for at least 1.5 h.

NH_4-MOR (Si/Al = 11.1, 0.5–10 g, CBV 21A, Zeolyst) was mixed with 1.5 L $NaNO_3$ solution (3.9×10^{-3}–1.2×10^{-2} M, Sigma–Aldrich) at 353 K for at least 12 h to exchange protons with sodium cations and then filtered and washed in 5 L deionized water to remove unexchanged Na^+. The washed sample was dried in ambient air at 363 K for at least 12 h and then treated in dry air (1.67 cm^3 s^{-1} at NTP conditions, ultrapure, Minneapolis Oxygen) at 773 K (0.0167 K s^{-1}) for 5 h.

Chemical titration using dimethyl ether (DME) for the H-FER, H-MOR, and H-BEA samples used in this study resulted in a DME per Al ratio of 0.5 ± 0.08 for all three zeolites, showing that the concentration of Brønsted acid sites is nearly identical to the concentration of Al in these materials. The experimental procedure and tabulated results of these DME titration studies are described in Supplemental information.

2.2. Steady-state catalytic reactions of n-hexane-hydrogen mixtures

Steady-state isomerization reactions of *n*-hexane were carried out in a tubular packed-bed quartz reactor (10 mm inner diameter) under atmospheric pressure and differential conditions (<8% for hydroisomerization). Catalyst samples were supported on a coarse quartz frit inside the reactor, and the temperature was controlled using a furnace (National Electric Furnace FA120 type) connected to a Watlow Temperature Controller (96 series). Catalyst temperatures were measured using a K-type thermocouple touching the bottom of a well on the external surface of the quartz reactor. Prior to measurement of *n*-hexane isomerization rates, catalyst samples (0.005–0.05 g proton form zeolites physically mixed with Pt/Al_2O_3 to achieve 0.9–1.0 Pt/H^+ molar ratio) were treated in H_2 at 673 K for 4 h (0.0167 K s^{-1}). When catalyst samples were insufficient in quantity to cover the thermowell, these samples were diluted with acid-washed quartz particles (0.5–0.8 g, 160–630 μm, European Commission, washed by 1 M HNO_3). Liquid *n*-hexane (4.6×10^{-5} mol s^{-1}) was vaporized at 383 K into a gas flow which contained He (1.8 cm^3 s^{-1} at NTP condition, Minneapolis oxygen), H_2 (0.15–1.75 cm^3 s^{-1}, ultra-pure carrier grade, Airgas), and a mixture of Ar/CH_4 (0.0137–0.0297 cm^3 s^{-1} at NTP conditions; 75% Ar and 25% CH_4, Minneapolis oxygen) as internal standard. The effluent from the reactor was sent via heated transfer lines to a mass

spectrometer (MKS Cirrus 200 Quadrupole mass spectrometer system) and a gas chromatograph (Agilent 6890N GC) equipped with a methyl-siloxane capillary column (HP-1, 50.0 m × 320 μm × 0.52 μm) connected to a flame ionization detector and a packed column (SUPELCO HAYESEP R 80/100 mesh packed column, 12 ft) connected to a thermal conductivity detector. Activation energies and pre-exponential factors were calculated from Arrhenius plots where the reaction rate constants were measured as a function of temperature (358–409 K).

3. Results and discussion

3.1. Mechanism and kinetics for n-hexane hydroisomerization over bifunctional catalysts

The mechanism for *n*-alkane hydroisomerization over bifunctional catalysts has been extensively studied in both experimental [12–14,16,18] and computational studies [24–26] to show that the mechanism involves (i) dehydrogenation of *n*-hexane (nC_6) to form *n*-hexene ($nC_6^=$) over platinum clusters (Scheme 1, Step 1), (ii) $nC_6^=$ adsorption on the zeolite acid site to form a surface-bound, linear alkoxide species (Scheme 1, Step 2), (iii) isomerization of this linear alkoxide species into a branched alkoxide species (Scheme 1, Step 3), (iv) desorption of the branched alkoxide to form a mono-branched alkene and concurrent regeneration of the zeolitic acid site (Scheme 1, Step 4), and (v) hydrogenation of the branched alkene on platinum clusters to generate mono-branched hexane (Scheme 1, Step 5).

The role of platinum in the bifunctional pathway of hydroisomerization was studied by Kondo et al. [18] using in situ infrared (IR) spectroscopy. The introduction of *n*-heptane and D_2 over platinum clusters supported on deuterated form of BEA zeolite (Pt/D-BEA) at 498 K resulted in the appearance of a broad band centered at 2170 cm^{-1} (C–D bond stretching) and the appearance of bands attributed to zeolitic OH groups (3600–3700 cm^{-1}) with the concurrent disappearance of bands attributed to zeolitic OD groups (2750 cm^{-1}), showing that there is H/D exchange between OD groups in Pt/D-BEA and the C–H bonds of *n*-heptane. No bands attributed to C–D bonds appeared in the infrared spectra using deuterated form of BEA (D-BEA without platinum) when *n*-heptane and D_2 were introduced as reactants under the same reaction conditions, suggesting that Pt promotes rapid H/D exchange on Pt/D-BEA. These observations support the hypothesis that Pt clusters catalyze the dehydrogenation of alkane reactants to form unsaturated alkenes which can undergo rapid H/D exchange with OD groups.

Demuth et al. [24] show using periodic DFT that for 2-pentene on ZSM-22, isomerization of an alkoxide species through an edge-protonated transition state has an activation energy of 110 kJ mol^{-1}; this energy barrier is higher than that required for chemisorption of the alkene reactant (52 kJ mol^{-1}). Their calculations also show that the activation energy required for isomerization of the surface-bound alkoxide through an edge-protonated transition state is considerably lower than that calculated for the isomerization reaction to occur via an alkyl shift transition state (180 kJ mol^{-1}), consistent with results presented by Boronat et al. [25]. Calculations done using cluster-based DFT or hybrid QM/MM methods show that the branched alkoxide species is less stable than the linear alkoxide species on 8T [27] and 46T [28] clusters of MFI and FAU [20], suggesting that the energy barrier for desorption of the branched alkoxide is lower than that for desorption of the linear alkoxide. Aronson et al. [29,30] observed rapid H/D exchange between C–H bonds of 2-methyl-2-propanol and D_2O using infrared spectroscopy and H-ZSM-5 catalysts at only 298 K, indicating the rate of adsorption and desorption of the branched alkoxide intermediate formed upon dehydration of the alcohol is fast. Therefore, in our reaction studies, desorption of branched hexoxide species (Scheme 1, Step 4) is unlikely to be the kinetically relevant step.

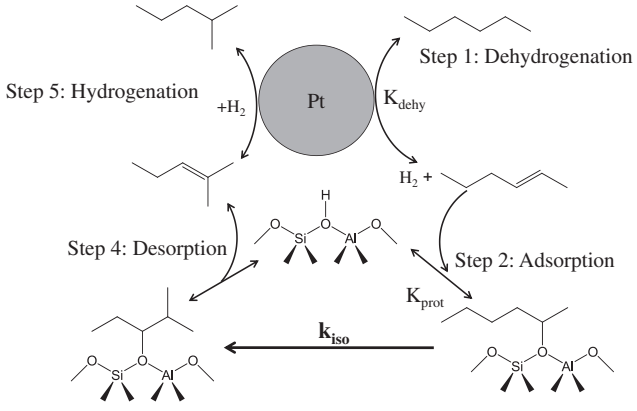

Scheme 1. Bifunctional mechanism for *n*-hexane hydroisomerization.

Eqs. (1) and (2) are the rate laws derived from the bifunctional hydroisomerization mechanism shown in Scheme 1 with the assumption that the surface is mainly occupied by surface-bound linear alkoxide species and empty Brønsted acid sites. In these two equations, K_{dehy} is the equilibrium constant for dehydrogenation of *n*-hexane on platinum surfaces (Step 1, Scheme 1); $K_{prot,2}$ and $K_{prot,3}$ are the equilibrium constants for formation of surface-bound 2-hexoxide and 3-hexoxide species by adsorption of *n*-hexene on Brønsted acid sites (Step 2, Scheme 1); K_{prot} is the equilibrium constant for formation of surface-bound hexoxide species including 1-hexoxide, 2-hexoxide, and 3-hexoxide, so $K_{prot} = K_{prot,1} + K_{prot,2} + K_{prot,3}$; k_{iso} is the rate constant for isomerization of surface-bound alkoxide species (Step 3, Scheme 1); $[H^+]_0$ is the number of initially accessible Brønsted acid sites; $[nC_6]$ is the partial pressure of *n*-hexane and $[H_2]$ is the partial pressure of hydrogen.

$$\frac{r_{2MP}}{[H^+]_0} = \frac{k_{iso,2}K_{prot,2}K_{dehy}\frac{nC_6}{H_2}}{1 + K_{prot}K_{dehy}\frac{nC_6}{H_2}} \quad (1)$$

$$\frac{r_{3MP}}{[H^+]_0} = \frac{k_{iso,3}K_{prot,3}K_{dehy}\frac{nC_6}{H_2}}{1 + K_{prot}K_{dehy}\frac{nC_6}{H_2}} \quad (2)$$

Eqs. (1) and (2) can be written in a linear form as Eqs. (3) and (4), which accurately describe the kinetic effects of H_2/n-C_6 molar ratio on the inverse rate of 2-methylpentane (2-MP) and 3-methylpentane (3-MP) formation over FER, MOR, and BEA as shown in Figs. 1–3b. The values of the apparent rate constant, $k_{app,2}$ ($k_{app,2} \equiv k_{iso,2}K_{prot,2}K_{dehy}$), and K_{prot} can be obtained from the values of the slope and the intercept, respectively. Using the values of $k_{app,2}$, K_{prot} obtained from Figs. 1–3b along with the value of K_{dehy}, which is calculated from thermochemical data [14], we can accurately predict the rates of *n*-hexane isomerization as shown in Figs. 1–3a. The isomerization rate over proton-form FER, MOR, and BEA can be described by the same rate equations (Eqs. (1) and (2)), suggesting that the same mechanism is operative on these materials under these reaction conditions. The isomerization rate is a function of n-C_6/H_2 molar ratio as shown in Figs. 1–3, consistent with the proposed bifunctional mechanism depicted in Scheme 1 where the concentration of $nC_6^=$ is in equilibrium with the n-C_6/H_2 molar ratio.

$$\frac{[H^+]_0}{r_{2MP}} = \frac{1}{k_{iso,2}K_{prot,2}K_{dehy}}\frac{[H_2]}{[nC_6]} + \frac{K_{prot}}{k_{iso,2}K_{prot,2}} \quad (3)$$

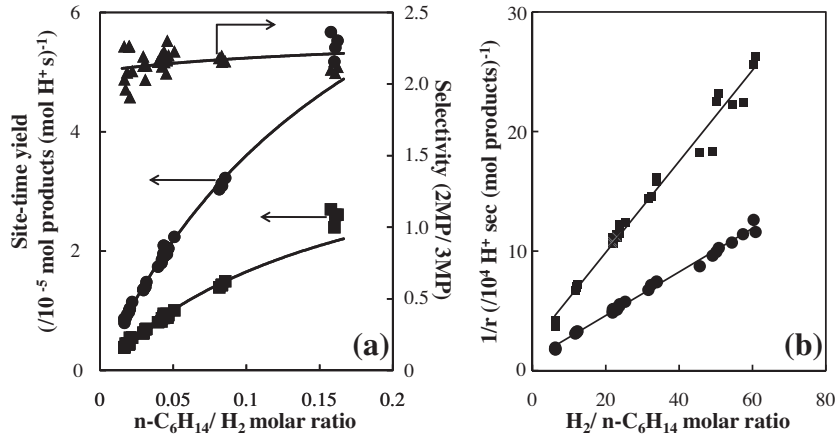

Fig. 1. (a) Measured site-time yield of 2-methylpentane (●), 3-methylpentane (■) and ratio of 2-methylpentane to 3-methylpentane rates as a function of n-C_6/H_2 molar ratio (▲) over FER at 473 K. The solid lines represent predictions from Eqs. (1) and (2). (b) Reciprocal rates of 2-methylpentane (●) and 3-methylpentane (■) as a function of H_2/n-C_6 molar ratio over FER at 473 K.

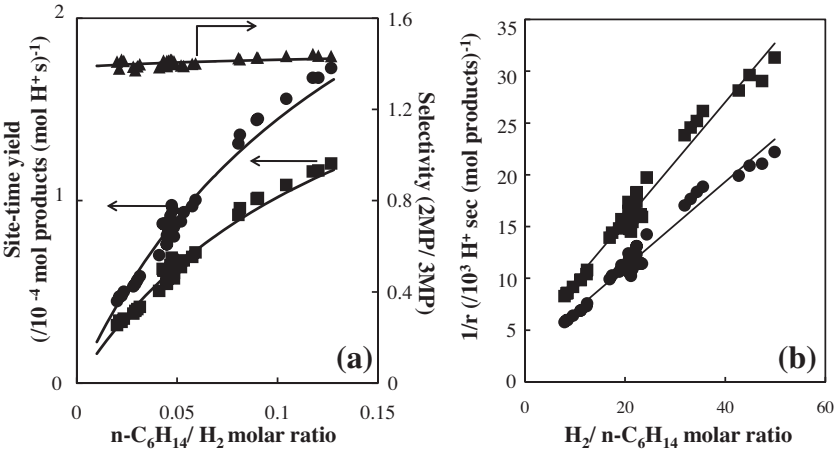

Fig. 2. (a) Measured site-time yield of 2-methylpentane (●), 3-methylpentane (■) and ratio of 2-methylpentane to 3-methylpentane rates as a function of n-C_6/H_2 molar ratio (▲) over MOR at 473 K. The solid lines represent predictions from Eqs. (1) and (2). (b) Reciprocal rates of 2-methylpentane (●) and 3-methylpentane (■) as a function of H_2/n-C_6 molar ratio over MOR at 473 K.

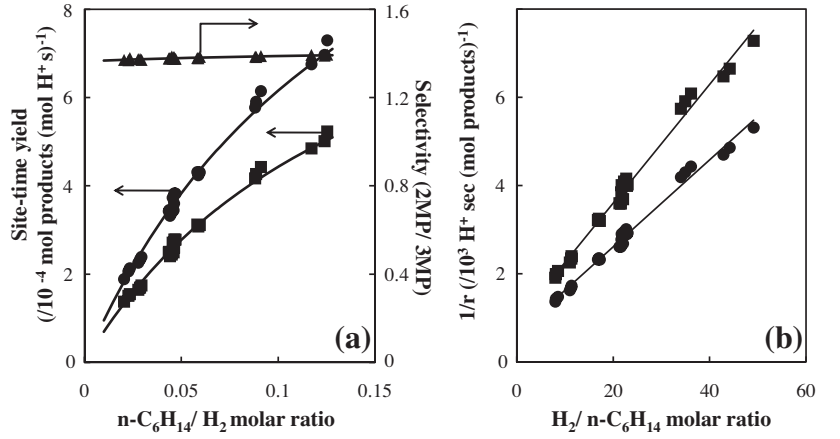

Fig. 3. (a) Measured site-time yield of 2-methylpentane (●), 3-methylpentane (■) and ratio of 2-methylpentane to 3-methylpentane rates as a function of n-C_6/H_2 molar ratio (▲) over BEA at 473 K. The solid lines represent predictions from Eqs. (1) and (2). (b) Reciprocal rates of 2-methylpentane (●) and 3-methylpentane (■) as a function of H_2/n-C_6 molar ratio over BEA at 473 K.

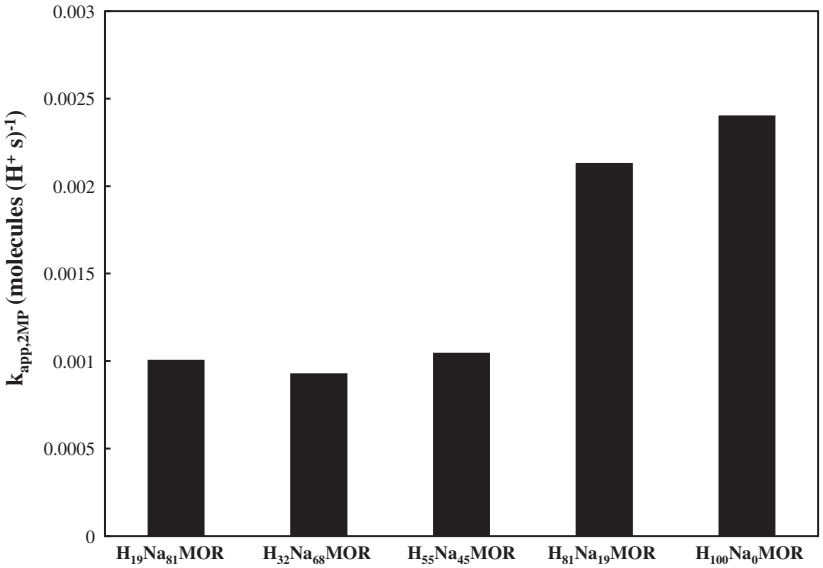

Fig. 4. Apparent rate constants of 2-methylpentane formation ($k_{app,2MP}$) over different sodium-exchanged MOR formulations at 473 K and nC_6/H_2 ratio = 0.02–0.14; H_xNa_{100-x} represents the fraction of OH groups in Na-exchanged MOR samples.

$$\frac{[H^+]_0}{r_{3MP}} = \frac{1}{k_{iso,3}K_{prot,3}K_{dehy}}\frac{[H_2]}{[nC_6]} + \frac{K_{prot}}{k_{iso,3}K_{prot,3}} \quad (4)$$

To eliminate the possibility of diffusion effects playing a significant role in the measured catalytic rates or selectivity on the zeolites studied, we calculated the effectiveness factor (η) according to the procedure reported by Haag et al. [4]. The calculated η is equal to 1 for both FER and MOR using the diffusion coefficient of *n*-hexane in FER (3.5×10^{-8}) and MOR (2.8×10^{-8}) calculated by Schuring et al. [31] using canonical (NVT) molecular dynamics simulations. Experimentally, de Gauw et al. [14] also concluded that no diffusion limitations exist for 12-MR BEA and MOR zeolites or for 10-MR MFI and TON materials for *n*-hexane hydroisomerization, because no effect on turnover frequency for MFI and TON and no effects on activation energy for BEA and MOR were noted with varying zeolite crystal size (0.6–3.5 μm for MFI, 1–4 μm for TON, 0.1–1 μm for BEA and 0.6–3.5 μm for MOR).

3.2. Assessment of the kinetics and rate of n-hexene isomerization in 8-MR side pockets and 12-MR channels within MOR using Na^+-exchanged samples

van de Runstraat et al. [13] suggested that two-thirds of the acid sites in MOR framework materials are inaccessible to *n*-hexane based on the observation that *n*-hexane adsorption capacity (0.07 ml g^{-1}) on their MOR-type material was only one-third of its BET volume (0.2 ml g^{-1}) and that the rate of *n*-hexane hydroisomerization on MOR per proton (9.7 mol mol^{-1} h^{-1}) was also ~1/3 of the rate on BEA (27.9 mol mol^{-1} h^{-1}) at 513 K. MOR consists of 12-MR main channels (denoted as MOR(12MR)) with intersecting 8-MR side pockets (denoted as MOR(8MR)) which may be inaccessible for *n*-hexane reactants due to the small pore opening (0.34×0.48 nm) [32]. Here, we used Na^+ to selectively replace the protons in 8-MR pockets of MOR to explore the accessibility of OH groups in 8-MR pockets for *n*-hexane reactions.

The asymmetric hydroxyl band corresponding to zeolitic OH groups (~3607 cm^{-1}) in the infrared (IR) spectrum of MOR can be deconvoluted to infer the existence of two distinct bands, one corresponding to OH groups in 8-MR pockets (3590 cm^{-1}) and the other corresponding to the OH groups in 12-MR channels (3610 cm^{-1}) [7,33]. Infrared spectra (shown in Fig. S.1 and reported in Table S.1 in the supplemental information) in the OH stretching region for H-MOR as Na^+ replaced some of the H^+ species show that the OH band in MOR became more symmetric with increasing Na^+ content because of a preferential weakening of the band corresponding to hydroxyl groups in 8-MR pockets implying that Na^+ selectively replaced H^+ in 8-MR pockets of MOR. Similar observations haves been reported by Veefkind et al. [34], Bhan et al. [7] and Maache et al. [35]. The number of H^+ in the 8-MR side pockets decreased ~50% when only ~20% of the total H^+ species were replaced in MOR. In contrast, the fraction of H^+ sites in 12-MR channels was largely unchanged by Na^+ when ~45% of the total H^+ sites were replaced in MOR.

The kinetics of *n*-hexane isomerization was measured on a series of Na^+-exchanged samples to show that k_{app} values for OH groups in 12-MR channels (9.3×10^{-4}–1.0×10^{-3} molecules $(H^+ s)^{-1}$) are nearly invariant with the concentration of OH groups ($H_{19}Na_{81}MOR$, $H_{32}Na_{68}MOR$ and $H_{55}Na_{45}MOR$) as shown in Fig. 4. The measured k_{app} of *n*-hexane hydroisomerization over samples containing OH groups in both 8-MR and 12-MR channels ($H_{81}Na_{19}$-MOR and $H_{100}Na_0MOR$) increased with the number of H^+ in the 8-MR pockets (Fig. 4), indicating that Brønsted acid sites circumscribed in the constrained 8-MR side pockets of MOR catalyze *n*-hexane isomerization with higher rates than acid sites circumscribed by larger 12-MR channels.

Eder et al. [36] showed that OH groups in 8-MR side pockets of MOR are not accessible to *n*-hexane based on the observation that the infrared band corresponding to OH groups in 12-MR channels of MOR decreased upon introduction of *n*-hexane, but the infrared band attributed to OH groups in 8-MR side pockets of MOR was nearly unperturbed even under 10 mbar of *n*-hexane at 303 K. In contrast, our results indicate that the OH groups in 8-MR pockets are accessible to *n*-hexene under hydroisomerization reaction conditions, suggesting that *n*-hexene is isomerized by the acidic OH groups contained within in 8-MR side pockets at high temperature (>473 K). Carpenter et al. [37] studied the constraint index (CI) of proton form MOR and sodium-exchanged MOR where the protons in 8-MR side pockets were selectively replaced by Na^+. Even though there was deactivation in both proton form MOR and sodium-exchanged MOR, they found that the CI value (~1.5) of sodium-exchanged MOR was constant with time-on-stream (TOS), while the CI value of proton form MOR increased from 1.5

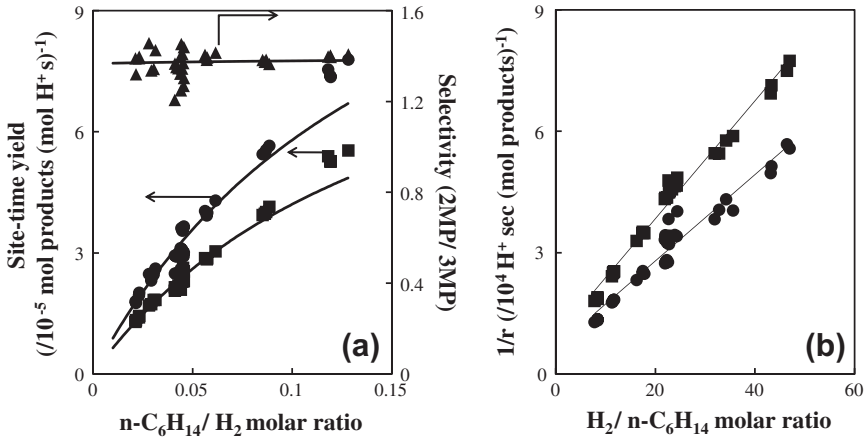

Fig. 5. (a) Measured site-time yield of 2-methylpentane (●), 3-methylpentane (■) and ratio of 2-methylpentane to 3-methylpentane rates as a function of n-C_6/H_2 molar ratio (▲) over $H_{32}Na_{68}$MOR at 473 K. The solid lines represent predictions from Eqs. (1) and (2). (b) Reciprocal rates of 2-methylpentane (●) and 3-methylpentane (■) as a function of H_2/n-C_6 molar ratio over $H_{32}Na_{68}$MOR at 473 K.

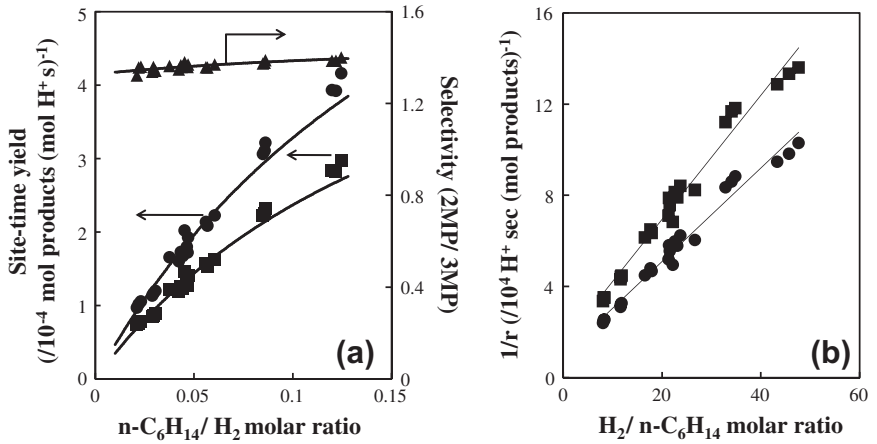

Fig. 6. (a) Calculated site-time yield of 2-methylpentane (●), 3-methylpentane (■) and ratio of 2-methylpentane to 3-methylpentane rates as a function of n-C_6/H_2 molar ratio (▲) in the 8-MR side pockets within MOR materials at 473 K. The solid lines represent predictions from Eqs. (1) and (2). (b) Reciprocal rates of 2-methylpentane (●) and 3-methylpentane (■) as a function of H_2/n-C_6 molar ratio in the 8-MR side pockets within MOR materials at 473 K.

Table 1
Rate constant of 2-methylpentane formation ($k_{app,2MP}$); ratio of rate constants for 2-methylpentane and 3-methylpentane formation ($k_{app,2MP}/k_{app,3MP}$) and apparent activation energy (E_{app}) and apparent entropy (ΔS_{app}) over proton form zeolite formulations.

Zeolite	$k_{app,2MP}$ at 473 K (molecules $(H^+ s)^{-1}$)	$k_{app,2MP}/k_{app,3MP}$ at 473 K	2-Methylpentane		3-Methylpentane	
			E_{app} (kJ mol^{-1})	ΔS_{app} (J mol^{-1} K^{-1})	E_{app} (kJ mol^{-1})	ΔS_{app} (J mol^{-1} K^{-1})
FER	5.4×10^{-4}	2.09	106.5 ± 3.6	−86.4 ± 7.4	123.2 ± 4.6	−86.4 ± 9.3
12MR-MOR	9.3×10^{-4}	1.50	128.0 ± 4.7	−37.4 ± 9.7	127.2 ± 3.5	−40.9 ± 7.3
8MR-MOR	4.9×10^{-3}	1.55	121.9 ± 4.7	−34.7 ± 9.8	123.1 ± 3.2	−35.0 ± 6.6
BEA	1.0×10^{-2}	1.35	117.1 ± 2.1	−33.1 ± 4.3	121.7 ± 3.0	−27.1 ± 6.1

to 6 with TOS at 603 K. These findings suggest that deactivation in 12-MR channels is faster than in 8-MR pockets and also show that n-hexane can enter the 8-MR side pockets of MOR at high temperatures relevant for hydrocarbon reactions on MOR.

The measured rate of isomerization per H^+ over the $H_{32}Na_{68}$-MOR sample is the rate per H^+ in the 12-MR channels of MOR, because only 12-MR channels have residual H^+ in this sample. The rate in the 8-MR pockets of MOR can be extracted by subtracting the rate in 12-MR channels of MOR from the rate in H-MOR. The measured rate of n-hexane isomerization in MOR(12MR) and the calculated rate in MOR(8MR) still follow Eqs. (1) and (2) as shown by the reciprocal rate plots in Figs. 5 and 6, respectively, indicating that the mechanism for n-hexane isomerization in MOR(8MR) and in MOR(12MR) can be accurately described by the bifunctional mechanism shown in Scheme 1. The k_{app} for olefin isomerization normalized per proton in the 8-MR pockets is five times larger than that in 12-MR channels of MOR as shown by the data reported in Table 1. These data constitute another example showing that catalytic turnover rates vary depending on the location of OH groups within a particular zeolite framework. Prior reports have discussed the specificity of OH groups in 8-MOR side pockets of H-MOR for CO insertion in surface methyl groups and monomolecular dehy-

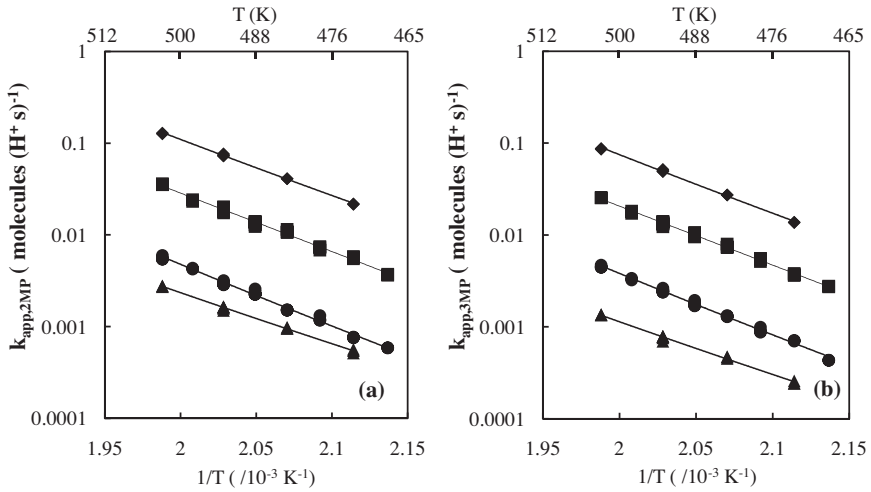

Fig. 7. Measured apparent rate constants of: (a) 2-methylpentane and (b) 3-methylpentane formation over BEA (♦), 8-MR pockets in MOR (■), 12-MR channels in MOR (●) and FER (▲) at *n*-C_6/H_2 ratio in the range 0.01–0.02.

drogenation of saturated hydrocarbons [7,8,38]. The detailed discussion of the essential role of local zeolite environment in enthalpic and entropic stabilization and in determining selectivity of isomerization reactions is presented in Section 3.4.

3.3. Effects of zeolite structure on n-hexane hydroisomerization

A comparison of kinetic and thermodynamic parameters assessed from linearized plots based on Eqs. (3) and (4) as shown in Figs. 1–3 for FER, MOR, and BEA is reported in Table 1. Rate constants for *n*-C_6 isomerization at 473 K increase in the order FER < MOR(12MR) < MOR(8MR) < BEA, consistent with reports in the literature where BEA has been reported to have a rate higher than MOR, MFI, and TON [13,39]. Regressed rate constants on acid sites in FER, BEA, MOR (12-MR) and MOR (8-MR) are shown as a function of temperature in Fig. 7; these data were used to estimate the apparent activation energy (E_{app}) and entropy (ΔS_{app}) for *n*-hexane hydroisomerization. The values of E_{app} and ΔS_{app} compiled in Table 1 represent the difference in energy and entropy between *n*-hexane in the gas phase and the transition state as shown in Scheme 2.

The apparent activation energy (E_{app}) of 2-MP formation decreases with decreasing the pore size as shown in Table 1. This trend may be caused by a decrease in the heat of physisorption (ΔH_{ads}) of linear hydrocarbons with increasing pore size [36,40–44], or caused by greater stabilization of electropositive transition states by negatively charged framework oxygen atoms in smaller channels as proposed by Rozanska et al. [45–47]. These authors studied the isomerization of toluene and xylene [47], cracking of thiophenic derivatives [46], and propylation of benzene [45] using periodic DFT methods and noted that cationic transition states are more stable when the electropositive hydrocarbon fragment is close to framework oxygen atoms and is surrounded by more framework oxygen atoms because of the partial negative charge on these oxygen atoms.

The measured activation energy, E_{app}, can be expressed as Eq. (5) according to the energy profile for *n*-hexane hydroisomerization as shown in Scheme 2, where ΔH_{dehy} is the enthalpy of *n*-hexane dehydrogenation (118 kJ mol^{-1}) [14], ΔH_{ads} is the heat of physisorption of *n*-hexene, ΔH_{alk} is the enthalpy of alkoxide formation by adsorption of *n*-hexene, and E_{int} is the intrinsic activation energy of alkoxide isomerization. The heat of physisorption of *n*-hexene can be estimated using the heat of *n*-hexane adsorption measured by Eder et al. [36,40] and Denayer et al. [43] with the consideration that physisorption energies arise primarily due to confinement and are largely independent of chemical functionality. If we subtract the contribution of ΔH_{dehy} and ΔH_{ads} from the E_{app}, the remaining values ($\Delta H_{alk} + E_{int}$) do not increase with decreasing pore size as shown in Table 2. Since E_{int} is likely to decrease with decreasing pore size due to electrostatic stabilization of the cationic transition state [45], this result may indicate that the stability of alkoxide intermediate is not only related to the diameter of a pore but also to the local environment of Brønsted acid site. This observation has been noted previously in computational studies by Boronat et al. [48] based on the remarkable changes in the energy for alkoxide formation from physisorbed 1-butene (from −14.5 kcal on 3T cluster to 7.1 kcal mol^{-1} on 11T

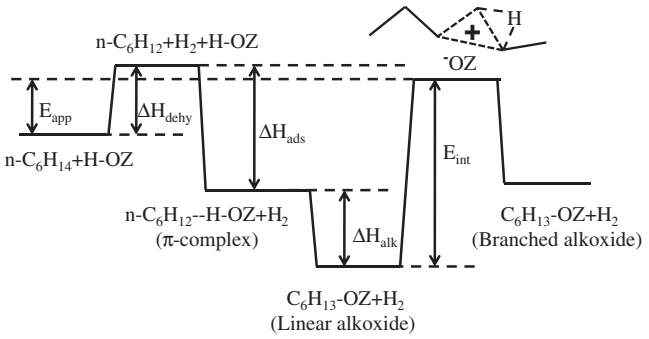

Scheme 2. Energy diagram for *n*-hexane hydroisomerization.

Table 2
Heat of adsorption of *n*-hexane (ΔH_{ads}), estimated energy difference between transition state and physisorbed hexene ($E_{int} + \Delta H_{alk}$) over proton form zeolite formulations.

Zeolite	ΔH_{ads} (kJ mol^{-1})	2-Methylpentane	3-Methylpentane
		$E_{int} + \Delta H_{alk}$ (kJ mol^{-1})	$E_{int} + \Delta H_{alk}$ (kJ mol^{-1})
FER	−79 [40]	67	84
12MR-MOR	−69 [36]	79	78
8MR-MOR	−92[a]	96	97
BEA	−63 [41]	62	66

[a] The heat of adsorption is estimated by assuming C_6 to be fully contained in the 8-MR pockets.

cluster for 2-butoxide formation) over four different clusters (3–26T atoms) cut from zeolite theta-1 using DFT (B3PW91) and Hartree–Fock (HF) methods. In another computational study, Rozanska et al. [49] studied the adsorption of propylene on zeolite CHA using periodic DFT (GGA) and their results show that the energy for alkoxide formation from physisorbed propylene changes from +23 kJ mol^{-1} to −27 kJ mol^{-1} upon increasing the flexibility of zeolite framework. These findings in the aforementioned computational studies also suggest that local geometry of zeolitic acid sites is an important parameter that determines the stability and reactivity of adsorbed hydrocarbon alkoxide species.

$$E_{app} = \Delta H_{dehy} + \Delta H_{ads} + \Delta H_{alk} + E_{int} \quad (5)$$

The rate of hydroisomerization on H-BEA catalysts is higher than that on FER and MOR materials due to the lower apparent activation energy in BEA compared to MOR and due to the higher activation entropy in BEA compared to FER. The higher entropy of activation in BEA than in FER is intuitively related to the large pore size of BEA and is consistent with the results reported by de Gauw et al. [14] for *n*-hexane hydroisomerization where they compare apparent rate constants for different zeolites and note that BEA has a larger pre-exponential factor than 10-MR zeolites ZSM-5 and ZSM-22.

Even though FER has the lowest E_{app}, it has the lowest reaction rate among the studied zeolites due to the larger entropy loss in FER compared to other zeolites studied as shown by the data reported in Table 1. The lowest ΔS_{app} and lowest E_{app} in FER are consistent with FER having smaller channels compared to MOR and BEA. FER has the highest $k_{app,2MP}/k_{app,3MP}$ ratio (2.1) among the zeolites studied, because FER has the largest difference in E_{app} between 3-MP formation and 2-MP formation (17 kJ mol^{-1} difference), in line with observations by van de Runstraat et al. [13] showing that 10-MR zeolites have a higher 2-MP/3-MP ratio (2.7–2.9 for TON and 3.4 for MFI) than 12-MR zeolites (1.5 for MOR and 1.6 for BEA), indicating that small pores put constraints on the formation of intermediates for 3-MP. The critical diameter for 2-MP and 3-MP is 0.54 nm [50,51] and the heats of physisorption of 2-MP and 3-MP are the same on 10-MR zeolites (62 kJ mol^{-1} for TON and 66 kJ mol^{-1} for MFI [43]), suggesting that the high $k_{app,2MP}/k_{app,3MP}$ observed in FER is not caused by any detectable differences in size or adsorption enthalpy of 2-MP and 3-MP and may instead be caused by differences in the stability of the alkoxide intermediate formed upon adsorption of the olefin or due to stabilization of the carbocationic transition state.

The data reported in Table 1 show that ΔS_{app}, E_{app}, $k_{app,2MP}/k_{app,3MP}$ of the MOR(8MR) are closer to values in large 12-MR channels of MOR and BEA instead of medium pore FER materials. The possible reasons for the 8-MR pockets in MOR behaving like 12-MR channels for *n*-hexane hydroisomerization reactions are discussed in Section 3.4.

3.4. Effects of partial confinement in 8-MR side pockets of MOR on n-hexane isomerization reactions

The size of 8-MR side pockets of MOR (0.34 × 0.48 nm) is smaller than the diameter of 12-MR channels of MOR (0.70 × 0.65 nm), whereas the values of ΔS_{app} for 2-MP and 3-MP formation in MOR(8MR) are similar to those in larger 12-MR channels of MOR and BEA as shown in Table 1. Webster et al. [52] calculated the dimensions of different molecules along *x*, *y*, and *z* axis using semi-empirical quantum chemistry methods, and the length of *n*-hexane (1.03 nm) they calculated is consistent with the length calculated by Jimenez-Cruz (1.06 nm) using DFT methods [51]. The depth of 8-MR pockets (∼0.37 nm) [8] is much shorter than the length of *n*-hexane [52,53]. Therefore, the similarity in ΔS_{app} measured for C_6 reactions in MOR(8MR), 12-MR channels of MOR, and BEA which is 46 J mol^{-1} K^{-1} higher than that measured in FER as shown in Table 1 may be caused by partial confinement effects first postulated by Gounder and Iglesia [8]. These authors showed that monomolecular alkane dehydrogenation was preferentially catalyzed by OH groups in 8-MR channels of MOR and that this specificity reflected transition states that were only partially confined within small 8-MR side pockets. This partial confinement resulted in entropic gains that compensated for enthalpic penalties incurred by incomplete containment within 8-MR pores and resulted in a lower overall free energy for monomolecular alkane cracking and dehydrogenation reactions. Carpenter et al. [37] suggested that the deactivation rate in 12-MR channels and 8-MR side pockets may be different based on the observation that the constraint index (CI) of proton form MOR increased from 1.5 to 6 with time-on-stream at 603 K. We note that the CI value is constant (CI = 6) after 5.2 h on proton form MOR, this value is much lower than the CI value in 8-MR zeolites (CHA > 100 and ERI = 38) [54], suggesting that OH groups in 8-MR pockets of MOR behave differently that OH groups in 8-MR channels of CHA and ERI for reactions of *n*-hexane and 3-methylpentane. The similar entropy loss for *n*-hexane hydroisomerization reactions for Brønsted acid catalytic centers circumscribed in 8-MR pockets and 12-MR channels of MOR and BEA, the length of the *n*-hexane molecule compared to the size of the 8-MR pocket in MOR, and the anomalous CI value of 8-MR channels in MOR lead us to hypothesize that the *n*-hexene molecule is partially confined in the 8-MR side pockets.

The transition state of hexene isomerization has a positively charged three-carbon ring (Scheme 2) which is expected to have a larger kinetic diameter than propane (0.43 nm) [8,52] based on their structures. Because it is difficult for the three-carbon ring (>0.43 nm) to be fully contained in the 8-MR pockets of MOR (0.34 × 0.48 nm), the three-carbon ring may be located near the pore mouth of the 8-MR pockets or in the 12-MR channels as shown in Scheme 3. The calculated 2-MP/3-MP selectivity in 8-MR pockets of MOR is similar to that in 12-MR channels of

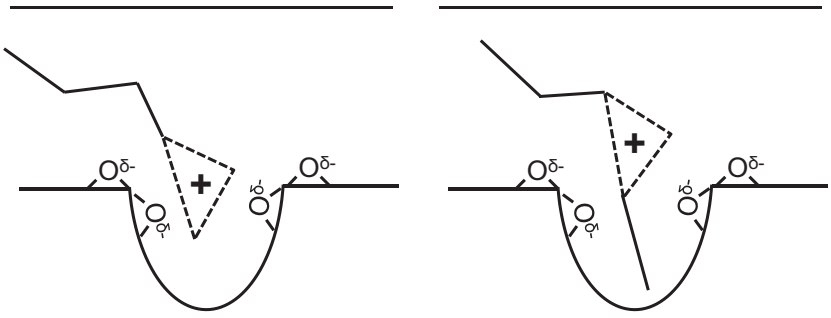

Scheme 3. The postulated cyclopropyl transition state for *n*-hexene isomerization in the 8-MR channels of MOR.

MOR and BEA but lower than that in FER as shown in Table 1, supporting our hypothesis that the 3-carbon ring is not completely contained within the 8-MR pockets of MOR.

The five fold larger rate in 8-MR side pockets compared to that in the 12-MR channels of MOR is a result of the lower activation energy in the 8-MR pockets. Rozanska et al. [47] studied isomerization of toluene and xylene and found that the CH_3^+ ion in the transition state of toluene isomerization is near the pore mouth of 8-MR side pockets in MOR such that it can be surrounded by more framework oxygen atoms even though the Brønsted acid site is located on the opposite side of these pore mouth oxygen atoms. We postulate that the cationic transition state of *n*-hexane isomerization may be located near the pore mouth of the 8-MR pockets and thereby be stabilized by framework oxygen atoms around the pore mouth of the 8-MR pockets which would result in a lower E_{app} in the 8-MR pockets compared to the 12-MR channels of MOR (Table 1). Pore mouth catalysis was first hypothesized by Martens et al. [55] to explain the high selectivity (~60%) for 2-methylnonane (2-MN) in decane hydroisomerization (2-MN/3-MN = 2.4) on 10-MR zeolite TON-type materials. They hypothesized that the reactant molecule is selectively adsorbed on the entrances of channels so that only part of the reactant is inside the channels, but the rest of the molecule is on the "external surface" of the zeolite crystal [5]. Our hypothesis is that *n*-hexene isomerization occurs at the pore mouth of 8-MR pockets in MOR and is an example of "intracrystalline" pore mouth catalysis where the reaction occurs at the pore mouth of one channel which intersects with a larger channel.

Clark et al. [32] showed that the adsorption of argon, methane, CF_4, and SF_6 in the 8-MR pockets of MOR is 5–8 kJ mol^{-1} stronger than in 12-MR channels of MOR using Grand Canonical Monte Carlo (GCMC) simulations. Therefore, another possible reason for the lower E_{app} in MOR(8MR) compared to that in MOR(12MR) is the larger heat of adsorption in smaller 8-MR pockets than in 12-MR channels mediated by confinement effects. The effective diameter of a pore is the average of the distances of the two axes of an elliptical pore after adding the oxygen atom diameter (0.27 nm) [8,56], and Savitz et al. [56] predicted the heat of adsorption of C_2–C_3 accurately using an effective pore diameter in a Lennard–Jones 12–6 potential. Because the effective pore radius of the small 8-MR pockets of MOR (0.34 nm) is close to the effective radii of the 10-MR channels (0.37 nm) and 8-MR channels (0.34 nm) in FER [8], the heat of alkane adsorption in FER can be used to approximate the heat of adsorption of hydrocarbons in the 8-MR pockets of MOR [8]. The depth of the 8-MR pockets (0.37 nm) is about 1/3 of the length of *n*-hexane (1.06 nm), so approximately two carbons can be accommodated in the 8-MR pocket. Therefore, the difference in the heat of *n*-hexane adsorption in 12-MR channels of MOR and *n*-hexane partially confined in 8-MR pockets can be estimated using the heats of ethane adsorption in the 12-MR channels of MOR and in FER. Eder et al. [36,40] measured the heat of adsorption of propane in MOR (-41 kJ mol^{-1}) and FER (-49 kJ mol^{-1}) and found that the heat of adsorption increases -9 kJ mol^{-1} and -10 kJ mol^{-1} per CH_2 group for C_3 to C_6 alkanes on MOR and FER, respectively. From these values, we estimate the heat of ethane adsorption in MOR (-32 kJ mol^{-1}) and FER (-39 kJ mol^{-1}). The difference between these two heats of adsorption (-7 kJ mol^{-1}) is similar to the difference in E_{app} for *n*-hexane isomerization between MOR(12MR) and MOR(8MR). Therefore, the lower E_{app} in MOR(8MR) compared to the E_{app} in MOR(12MR) may be due to the larger heat of adsorption caused by the partial confinement of *n*-hexane in 8-MR side pockets.

The enhancement in the rate of *n*-hexane hydroisomerization in the 8-MR pockets of MOR is in line with recent reports demonstrating selective CO insertion into surface-bound methoxide species [6,7,10], higher rates for monomolecular cracking and dehydrogenation of propane and butane [8,9], and selective unimolecular ethanol dehydration [11]. Collectively, these reports and our work for *n*-hexane hydroisomerization described above show that the location of zeolitic OH groups strongly influences reaction rates and selectivity. The selectivity for 2-MP/3-MP and the entropy of reaction for 2-MP and 3-MP formation in 8-MR side pockets of MOR is similar to that in 12-MR channels of MOR and BEA instead of medium pore FER, showing that pore size cannot be used to accurately predict the occurrence or exclusion of a particular reaction within zeolitic solids. Our findings regarding intracrystalline pore mouth catalysis provide another conceptual consideration for rigorous and quantitative understanding of local environment effects of zeolite channel size and connectivity on the rate and selectivity of acid-catalyzed reactions.

4. Conclusions

n-C_6H_{14} hydroisomerization reactions showed that measured rates of 2-methylpentane (2MP) and 3-methylpentane (3MP) formation were linearly proportional to the molar ratio of H_2 to *n*-C_6H_{14} over FER, MOR, and BEA zeolites, consistent with a bifunctional mechanism involving the facile dehydrogenation of *n*-hexane on the metal catalyst and a kinetically relevant step involving isomerization of *n*-hexene on zeolitic acidic sites. The rate of *n*-hexane hydroisomerization increases in the order FER < MOR(12MR) < MOR(8MR) < BEA. The measured temperature dependence of hydroisomerization rates showed that the low isomerization rates in FER are primarily a result of entropy loss.

Na^+ selectively replaced protons within 8-MR pockets of MOR and led to a disproportionate decrease in hexane isomerization turnover rates per H^+, showing that the rate of *n*-hexane hydroisomerization in 8-MR pockets is five times larger than the rate in 12-MR channels of MOR. The similar entropy loss in small 8-MR channels compared to larger 12-MR channel in MOR is consistent with a partial confinement hypothesis, where adsorbates and activated complexes are only partially confined in the small 8-MR side pockets of MOR. The bulky 3-carbon ring of the cationic transition state may be located near the pore mouth, resulting in similar selectivity of 2MP to 3MP but lower apparent activation energy compared to 12-MR channels of MOR due to electrostatic stabilization by negatively charged framework oxygen atoms around the pore mouth of the 8-MR pockets or due to the partial adsorption in 8-MR pockets.

A positively charged transition state, reactant, or intermediate located at the pore mouth of small zeolitic channels can optimize its free energy by partially protruding into the large channels in order to gain entropy and release energy through stronger dispersion forces or electronic stabilization as a result of partial confinement by the pore mouth of small channels. The concepts of intracrystalline pore mouth catalysis provide another fundamental consideration for zeolite-catalyzed reactions when the dimensions of a reactant or intermediate are larger than the dimension of a small channel intersecting with a larger channel.

Acknowledgments

The authors acknowledge the financial support from ARPA-E program (ARPA-E, Award number # DE-AR0000007). H.C. was partially supported by funds from the Petroleum Institute of Abu Dhabi through the ADMIRE (Abu Dhabi-Minnesota Institute for Research Excellence) partnership. Sasol North America Inc. donated Al_2O_3 samples. We acknowledge Dr. Do-Young Hong for the preparation and characterization of Na^+-MOR samples and also thank Mingwei Tian, Henry Kim, and Yasser Al Wahedi for assistance with the synthesis of Pt/Al_2O_3.

Appendix A. Supplementary material

Supplementary data associated with this article can be found, in the online version, at doi:10.1016/j.jcat.2011.07.006.

References

[1] M. Brandle, J. Sauer, J. Am. Chem. Soc. 120 (1998) 1556–1570.
[2] C. Lo, B.L. Trout, J. Catal. 227 (2004) 77–89.
[3] P.B. Weisz, Pure Appl. Chem. 52 (1980) 2091–2103.
[4] W.O. Haag, R.M. Lago, P.B. Weisz, Faraday Discuss. 72 (1981) 317–330.
[5] T.F. Degnan, J. Catal. 216 (2003) 32–46.
[6] A. Bhan, E. Iglesia, Acc. Chem. Res. 41 (2008) 559–567.
[7] A. Bhan, A.D. Allian, G.J. Sunley, D.J. Law, E. Iglesia, J. Am. Chem. Soc. 129 (2007) 4919–4924.
[8] R. Gounder, E. Iglesia, J. Am. Chem. Soc. 131 (2009) 1958–1971.
[9] R. Gounder, E. Iglesia, Angew. Chem. – Int. Edit. 49 (2010) 808–811.
[10] P. Cheung, A. Bhan, G.J. Sunley, D.J. Law, E. Iglesia, J. Catal. 245 (2007) 110–123.
[11] H. Chiang, A. Bhan, J. Catal. 271 (2010) 251–261.
[12] J. Macht, R.T. Carr, E. Iglesia, J. Am. Chem. Soc. 131 (2009) 6554–6565.
[13] A. van de Runstraat, J.A. Kamp, P.J. Stobbelaar, J. van Grondelle, S. Krijnen, R.A. van Santen, J. Catal. 171 (1997) 77–84.
[14] F. de Gauw, J. van Grondelle, R.A. van Santen, J. Catal. 206 (2002) 295–304.
[15] P.B. Weisz, E.W. Swegler, Science 126 (1957).
[16] H.Y. Chu, R.P. Rosynek, J.H. Lunsford, J. Catal. 178 (1998) 352–362.
[17] B. Xu, C. Sievers, S.B. Hong, R. Prins, J.A. van Bokhoven, J. Catal. 244 (2006) 163–168.
[18] J.N. Kondo, S.W. Yang, Q.J. Zhu, S. Inagaki, K. Domen, J. Catal. 248 (2007) 53–59.
[19] V. Nieminen, M. Sierka, D.Y. Murzin, J. Sauer, J. Catal. 231 (2005) 393–404.
[20] B.A. De Moor, M.F. Reyniers, G.B. Marin, Phys. Chem. Chem. Phys. 11 (2009) 2939–2958.
[21] W. Wang, J. Jiao, Y.J. Jiang, S.S. Ray, M. Hunger, ChemPhysChem 6 (2005) 1467–1469.
[22] T. Blasco, Chem. Soc. Rev. 39 (2010) 4685–4702.
[23] Y.J. Jiang, M. Hunger, W. Wang, J. Am. Chem. Soc. 128 (2006) 11679–11692.
[24] T. Demuth, X. Rozanska, L. Benco, J. Hafner, R.A. van Santen, H. Toulhoat, J. Catal. 214 (2003) 68–77.
[25] M. Boronat, P. Viruela, A. Corma, J. Phys. Chem. 100 (1996) 16514–16521.
[26] A.L.L. East, T. Bucko, J. Hafner, J. Phys. Chem. A 111 (2007) 5945–5947.
[27] H.J. Fang, A.M. Zheng, S.H. Li, J. Xu, L. Chen, F. Deng, J. Phys. Chem. C 114 (2010) 1054–10264.
[28] S. Namuangruk, D. Tantanak, J. Limtrakul, J. Mol. Catal. A: Chem. 256 (2006) 113–121.
[29] M.T. Aronson, R.J. Gorte, W.E. Farneth, D. White, J. Am. Chem. Soc. 111 (1989) 840–846.
[30] M.T. Aronson, R.J. Gorte, W.E. Farneth, J. Catal. 105 (1987) 455–468.
[31] D. Schuring, A.P.J. Jansen, R.A. van Santen, J. Phys. Chem. B 104 (2000) 941–948.
[32] L.A. Clark, A. Gupta, R.Q. Snurr, J. Phys. Chem. B 102 (1998) 6720–6731.
[33] M.A. Makarova, A.E. Wilson, B.J. van Liemt, C. Mesters, A.W. de Winter, C. Williams, J. Catal. 172 (1997) 170–177.
[34] V.A. Veefkind, M.L. Smidt, J.A. Lercher, Appl. Catal. A 194 (2000) 319–332.
[35] M. Maache, A. Janin, J.C. Lavalley, E. Benazzi, Zeolites 15 (1995) 507–516.
[36] F. Eder, M. Stockenhuber, J.A. Lercher, J. Phys. Chem. B 101 (1997) 5414–5419.
[37] J.R. Carpenter, S. Yeh, S.I. Zones, M.E. Davis, J. Catal. 269 (2010) 64–70.
[38] P. Cheung, A. Bhan, G.J. Sunley, E. Iglesia, Angew. Chem. – Int. Edit. 45 (2006) 1617–1620.
[39] T. Yashima, Z.B. Wang, A. Kamo, T. Yoneda, T. Komatsu, Catal. Today 29 (1996) 279–283.
[40] F. Eder, J.A. Lercher, J. Phys. Chem. B 101 (1997) 1273–1278.
[41] J.F. Denayer, G.V. Baron, J.A. Martens, P.A. Jacobs, J. Phys. Chem. B 102 (1998) 3077–3081.
[42] C.E. Ramachandran, B.A. Williams, J.A. van Bokhoven, J.T. Miller, J. Catal. 233 (2005) 100–108.
[43] J.F. Denayer, W. Souverijns, P.A. Jacobs, J.A. Martens, G.V. Baron, J. Phys. Chem. B 102 (1998) 4588–4597.
[44] B.A. De Moor, M.F. Reyniers, O.C. Gobin, J.A. Lercher, G.B. Marin, J. Phys. Chem. C 115 (2011) 1204–1219.
[45] X. Rozanska, L. Barbosa, R.A. van Santen, J. Phys. Chem. B 109 (2005) 2203–2211.
[46] X. Rozanska, R.A. van Santen, F. Hutschka, J. Hafner, J. Catal. 215 (2003) 20–29.
[47] X. Rozanska, R.A. van Santen, F. Hutschka, J. Hafner, J. Am. Chem. Soc. 123 (2001) 7655–7667.
[48] M. Boronat, C.M. Zicovich-Wilson, P. Viruela, A. Corma, J. Phys. Chem. B 105 (2001) 11169–11177.
[49] X. Rozanska, T. Demuth, F. Hutschka, J. Hafner, R.A. van Santen, J. Phys. Chem. B 106 (2002) 3248–3254.
[50] C.L. Cavalcante, D.M. Ruthven, Ind. Eng. Chem. Res. 34 (1995) 177–184.
[51] F. Jimenez-Cruz, G.C. Laredo, Fuel 83 (2004) 2183–2188.
[52] C.E. Webster, R.S. Drago, M.C. Zerner, J. Am. Chem. Soc. 120 (1998) 5509–5516.
[53] I. Daems, R. Singh, G. Baron, G. Denayer, Chem. Commun. (2007) 1316–1318.
[54] S.I. Zones, T.V. Harris, Microporous Mesoporous Mater. 35 (6) (2000) 31–46.
[55] J.A. Martens, R. Parton, L. Uytterhoeven, P.A. Jacobs, G.F. Froment, Appl. Catal. 76 (1991) 95–116.
[56] S. Savitz, F. Siperstein, R.J. Gorte, A.L. Myers, J. Phys. Chem. B 102 (1998) 6865–6872.